Journal of Controlled Release 145 (2010) 231–239

Contents lists available at ScienceDirect

Journal of Controlled Release

journal homepage: www.elsevier.com/locate/jconrel

Slow and sustained release of active cytokines from self-assembling peptide scaffolds

Fabrizio Gelain [a,d,*,1], Larry D. Unsworth [b,c,1], Shuguang Zhang [d,*]

[a] Center for Nanomedicine and Tissue Engineering, Pad. Mariani A.O. Ospedale Niguarda Ca' Granda Piazza dell'ospedale maggiore 3, Milan, 20162, Italy
[b] Department of Chemical and Materials Engineering, University of Alberta, ECERF 7-070D, 9107-116 St., Edmonton, Alberta, Canada T6G 2V4
[c] National Institute for Nanotechnology, National Research Council, 11421 Saskatchewan Drive, Edmonton, Alberta, Canada T6G 2V4
[d] Center for Biomedical Engineering, Massachusetts Institute of Technology, NE47-379, 77 Massachusetts Avenue, Cambridge, MA 02139-4307, USA

ARTICLE INFO

Article history:
Received 29 January 2010
Accepted 26 April 2010
Available online 4 May 2010

Keywords:
Cytokines
Drug release
Neural stem cells
Self-assembling peptides

ABSTRACT

Controlling the cellular microenvironment is thought to be critical for the successful application of biomaterials for regenerative medicine strategies. Self-assembling peptides are proving to be a promising platform for a variety of regenerative medicine applications. Specifically, RADA16-I self-assembling peptides have been successfully used for 3D cell culture, accelerated wound healing, and nerve-repair. Understanding the fundamental mechanisms for protein mobility within, and ultimately release from, this nanostructured system is a critical aspect for controlling cellular activity; studies which are largely lacking within the literature. Herein, we report that designer self-assembling peptide scaffolds facilitate slow and sustained release of active cytokines that are extremely relevant to many areas of regenerative medicine. In addition, multiple diffusive mechanisms are observed to exist for human βFGF, VEGF and BDNF within RADA16-I and two different RADA16-I nanofiber forming peptides with net positive or negative charges located at the C-terminus. In some cases, two populations of diffusing molecules are observed at the molecular level: one diffusing fully within the solvent, and another that exhibits hindered mobility. Results suggest that protein mobility is inhibited by both physical hinderances and charge induced interactions between the protein and peptide nanofibers. Moreover, assays using adult neural stem cells (NSCs) are employed to assess the functional release of active cytokine (βFGF) up to three weeks. Our results not only provide evidence for long-term molecular release from self-assembling peptide scaffolds but also inspiration for a plethora of slow molecular release strategies for clinical applications.

© 2010 Elsevier B.V. All rights reserved.

1. Introduction

Facilitating advantageous cellular activity through controlling the local cues within the cellular microenvironment is the ultimate goal of the majority of regenerative medicine studies. Hydrogels that are amenable to non-invasive therapies have long been recognized as being crucial to regenerative medicine efforts [1–3]. Recently, it has been shown that hydrogels formed from self-assembling peptides (RADA16-I) have attributes that make them ideal for soft-tissue applications [4,5]: generally non-immunogenic, lacking an inflammatory response, non-thrombogenic, applicable to non-invasive therapies (i.e. void filling), gel under physiological conditions, stimulates cellular response *via* a 3-D microenvironment, while maintaining an internal hydration of up to 99.5% (w/v) water [6–10]. For these reasons, self-assembling peptides have gained acceptance as scaffolds for 3-D cell culturing systems [11–13], regenerative medicine applications [10,14], and drug delivery applications [9,15,16]. It is thought that the biocompatible traits of RADA16-I, coupled with the ease of peptide functionalization, should allow for the development of novel cell based therapies [11]. Utilization of these materials for regenerative [9] medicine purposes necessitates the controlled presentation of therapeutically relevant proteins for directing cellular activity; where it is generally agreed that hydrogels used for regenerative medicine strategies should be capable of modulating the mobility of bioactive proteins as a means of altering their presentation to local cells [15].

The programmability of the amino acid sequence of these self-assembling proteins allows a means of controlling and fine-tuning nanofiber properties at the molecular level. This programmability may provide a platform from which peptide engineering may significantly affect molecular diffusion. However, despite the recognized importance of incorporating and controlling the release of therapeutically relevant biomacromolecules including cytokines, very little work has focused on understanding the crucial role that the physicochemical properties of these nanofibers have on influencing the release mechanism, release rate, solution protein conformation and protein function. This information is of fundamental importance,

* Corresponding authors. Gelain is to be contacted at Center for Nanomedicine and Tissue Engineering, Pad. Mariani A.O. Ospedale Niguarda Ca' Granda Piazza dell'ospedale maggiore 3, Milan, 20162, Italy. Tel.: +39 02 6444 3245; fax: +39 02 6444 3258. Zhang, Tel.: +1 617 258 7514; fax: +1 617 258 5239.
E-mail addresses: gelain@mit.edu (F. Gelain), shuguang@mit.edu (S. Zhang).
[1] These authors contributed equally to this work.

0168-3659/$ – see front matter © 2010 Elsevier B.V. All rights reserved.
doi:10.1016/j.jconrel.2010.04.026

as protein diffusion through hydrogels may not only affect host tissue events at the implantation site but may also dictate cellular events within the construct itself (e.g. gene expression, stem cell differentiation, etc.). Some examples of protein release from these designed peptide scaffolds include the *in vivo* delivery of IGF from biotinylated RADA16-I nanofibers, which yielded a slow release of IGF-1 upon being implanted within the infarcted myocardia of rats [15]. Small molecule releases from these self-assembled scaffolds were shown to be affected by nanofiber backbone charge [9,16]. For unmodified RADA16-I systems [17], a clear relationship between protein release kinetics and nanofiber density, relative to protein dimension, was previously demonstrated. Herein we attempt to elucidate the effect of nanofiber charge upon the mobility of similar sized proteins of different isoelectric points. Moreover, cellular activity studies are conducted to investigate the period of functional release of cytokines that occurs from these systems. It is hoped that coupling the in-gel dynamics of protein mobility with functional release studies will allow for further engineering of these nanofiber scaffolds so as to augment cellular activity.

To this end, we selected several cytokines, of similar molecular weight (Table 1) but differing isoelectric points, to incorporate into 3 hydrogel scaffolds: a) RADA16-I (Ac-RADARADARADARADA-$CONH_2$), b) RADA16-DGE (Ac-RADARADARADARADAGGDGEA-$CONH_2$) and c) RADA16-PFS (Ac-RADARADARADARADAGGPFSSTKT-$CONH_2$) that have net charges of neutral, negative and positive at a solution pH of 17.4, respectively. Basic-fibroblast cytokine (βFGF, +), vascular endothelial cytokine (VEGF, −) and brain-derived neurotrophic factor (BDNF, +) were used as molecular probes because: 1) they had similar sizes but overall charge differences; 2) cell function assays were generally available and 3) they are used in a number of *in vitro* tests and *in vivo* experimental therapies [18,19]. Thus, it is thought that these cytokines would provide evidence that adding negatively or positively charged domains to RADA16-I would effectively modulate their release from these hydrogels.

Despite the intense effort expended upon determining the rate of protein mobility within various biomaterial constructs, most employ the 1-D unsteady-state form of Fick's second law [21–23]. The widespread application of which is problematic given the constraints that net diffusion is considered concentration independent and that there is an absence of solute–material interactions [24,25]. The latter being reported as being involved in altering the mobility of difusing solutes in several articles looking at diffusion within peptide based hydrogels, which utilize this unsteady-state Fickian model [26,27]. Neither simple bulk measurements of molecular release kinetics into solution [28] nor even more sophisticated methods like fluorescence recovery after photobleaching (FRAP) can provide a means of determining population distributions of molecular mobility within hydrogel materials [26]. To address this shortcoming, recent work has focused on using 'single-molecule' fluorescence correlation spectroscopy (FCS) approach that allows for the experimental determination of the diffusion properties of in-gel proteins [17]. This technique allows for the characterization of diffusion parameters for different sub-populations of a single protein population within the nanofiber matrix. The theory of which has been discussed in detail elsewhere [29–31].

The results we obtained suggest that the charged residues added to the carboxyl-termini of RADA16-I influence cytokine–nanofiber interactions, altering their release kinetics. In general, two populations of diffusing molecules were identified, one being attributed to the diffusion of molecules in the large aqueous 'void' of the 1% (w/v) peptide nanofiber scaffold and the other a population of cytokines that are impeded *via* an interaction with the nanofiber scaffold. It is likely that the slower population of diffusing molecules may allow for the long-term delivery of cytokines, which were observed to influence cells *in vitro* for several weeks. Here, we observed that electrostatic differences between the nanofiber and the cytokine had an effect on their mobility, suggesting that inhibition of cytokine mobility within the hydrogel was not only due to the physical presence of the nanofibers, but also was affected by nanofiber charge. To our knowledge, this is one of the first studies to characterize systematically the diffusive characteristics of multiple populations of a single cytokines within a nanofiber scaffold. It is thought that this information will allow for the design of cellular microenvironments for many regenerative medicine applications.

Table 1
Physicochemical properties for all proteins and self-assembling peptides, including net charge, molecular weight (MW), and solution diffusivity. pI was calculated using amino acid pK values as described elsewhere [20]. Solution diffusivity was measured using fluorescent correlation spectroscopy methods, with protein concentrations between 14 nM and 0.5 nM.

	pIl, exp'1, calc'd	Net charge, pH 7.4	MW,[a] Da	Solution diffusity,[b] $\times 10^{10} m^2/s$
Protein				14–0.5 nM
βFGF	10.03, 9.59	+	17,100	1.4–2.2 (±0.1)
BDNF	9.99, 9.59	+	27,000	1.8–2.1 (±0.1)
VEGF	n/a, 7.2	−	38,200	1.6–2.2 (±0.1)
Matrix				
RADA16-I	7.4, 8.1	Neutral	1713	
RADA16-DGE	n/a, 4.2	−	2199	
RADA16-PFS	n/a, 11.1	+	2576	

[a] GF molecular weight as provided by supplier.
[b] As measured using FCS techniques, $n = 5$ for all protien concentrations.

2. Materials and methods

2.1. Self-assembling peptide synthesis and cytokine labeling

The self-assembling peptides RADA16-I, RADA16-PFS and RADA16-DGE were synthesized using a CEM liberty microwave automated synthesizer. Sample masses were characterized *using* MALDI-TOF mass-spectrometer (Applied Biosystems), HPLC purified to greater than 95% (results not shown) (Waters), lyophilized (Labconco) and dissolved at 1% concentration ((w/v) in distilled water, pH ~ 3). Neutral pH7.4, phosphate buffered (PB) solutions were prepared by adding specific amounts of Monosodium phosphate (Sigma), monohydrate and Disodium phosphate, heptahydrate (Sigma) to distilled water. Cytokines (human recombinant BDNF, human recombinant βFGF and human recombinant VEGF121) were purchased from Peprotech (Rocky Hill, New Jersey) and used without further purification. Alexa Fluor® 647 Microscale Protein Labeling Kit was purchased from Molecular Probes (Carlsbad, California), and used to label the cytokines: un-reacted dyes were removed from the reaction mixture *via* centrifugation.

2.2. Diffusion experiments experimental setup

Labeled and unlabelled protein concentrations were measured by a NanoDrop Spectrophotometer (NanoDrop Technologies). The final concentration of the self-assembling peptides was 0.9% (w/v) while, within gel solutions labeled and unlabeled protein concentrations were 5 nM and 50 nM respectively. These solutions were used for all fluorescent correlation spectroscopy (FCS) experiments, which were carried out at room temperature (RT) using the MF-20 (Olympus, Japan). Peptide–protein solutions were placed in 384-multiwell glass microplate (20 μL per well) and 180 μL of buffer was slowly added so as to accelerate peptide self-assembly. Protein release experiments were performed at RT, where supernatants (100 μL) were sampled at 0.5, 1, 2, 3, 5, 8, 24, 30 and 48 h. Sampled supernatant was replaced by

fresh buffer. These data points allowed for the direct determination of released protein amounts as a function of time. It should be mentioned that due to the fact that there may exist an interaction between the diffusant and the nanofibers, diffusivities calculated using bulk release techniques yield apparent diffusivities and are for comparison purposes only: between both different systems and values determined using FCS characterization techniques. Moreover, FCS techniques were used to characterize cytokine diffusion within the self-assembled peptide scaffold and supernatants at selected time points. Although several algorithms have been developed to analyze the autocorrelation function for anomalous diffusion cases [32–34], the equipment used in our experiments (Olympus MF-20) did not allow for the fitting of the data in this manner. Moreover, this equipment did not allow for the capture of the raw autocorrelation data, thus other algorithms could not be employed to characterize these data.

2.3. In vitro βFGF release: neural stem cell proliferation test

Adult mouse neural stem cell (NSC) cultures were established and expanded as previously described [11]. NSCs were seeded at a concentration of 20×10^3 cells/well of a 24-multiwell plate (BD Falcon, San Jose, US) two days after the last mechanical dissociation in order to seed the maximum percentage of stem cells. Standard NSC culture medium deprived of cytokines was used for the experiment (500 μL per well). Peptide solutions 1% (v/w) were mixed with βFGF solutions (1:40 ratio): final cytokine concentration within gel was 100 nM. As the purpose for these experiments was to investigate functionality of released βFGF, this concentration was chosen in order to maintain a working dilution (1:12 between scaffolds and cell culture media) of the fraction of βFGF released in the media capable of stimulating NSC proliferation over multiple weeks (as an example the concentration ordinarily used with NSC expansion cultures is 20 ng/mL) [35]. An aliquot of 40 μL of gel and βFGF solution was applied to cell culture inserts membranes (1 μm pore size; Falcon) and allowed to self-assemble in wells filled with PBS (7.4 pH) for 30 min: for negative controls empty inserts were used. Inserts with scaffolds were placed in wells with NSCs. Culture experiments continued for four weeks, where cell proliferation was assessed weekly using MTT assay (see next paragraph) while inserts with scaffolds were placed in new wells with PBS first for washing from previous medium then in wells with same initial concentration of NSCs and fresh medium.

2.4. Cell imaging and proliferation assay

Cell imaging was performed using an inverted microscope (Zeiss) one week after seeding. To assess the viability of proliferated cells upon exposure to released βFGF from peptide scaffolds, a quantitative method, MTT assay (Sigma), was used. MTT (3-(4,5-dimethylthiazol-2yl)-2,5 diphenyl tetrazolium bromide) was prepared in a 5 mg/mL stock solution in PBS, then added to the culture medium in a ratio of 1:100. After an hour of incubation at +37 °C, the MTT solution was removed and the insoluble formazan crystals were dissolved by soaking scaffolds and cells for 15 min in 250 μL of dimethylsulfoxide (DMSO). The absorbance was measured by using a Versamax microplate reader (Molecular Devices, Sunnyvale CA) at an absorption wavelength of 550 nm. For the cell viability test the direct proportional linearity between the optical density and the viability/metabolic activity of the cell populations was assessed by verifying the linearity of 5 different standard curves at 6 increasing cell concentrations, ranging from 2×10^3 to 2×10^5 cells/well. Results are expressed as arbitrary absorbance units (a.a.u.).

3. Results and discussion

We have reported previously that RADA16-I [17] and RADA16-PFS [11,36] peptides (Table 1) self-assemble into nanofibers upon exposure to neutral pH solutions [11]. Using similar techniques, RADA16-DGE has been shown to self-assemble into nanofibers (see Supplementary data). While single fiber thickness may slightly vary between these three constructs by a few nanometers, when 6 and 9 amino acids appended to RADA16 [36], it is expected that this does not alter significantly the pore size distribution between the various nanofiber systems that may influence the in-gel mobility of proteins. This is especially apparent when one considers the large fraction of water (~99%) within these hydrogels themselves.

3.1. Apparent diffusivity and plateau release kinetics: solution data

Cytokine release profiles for all peptide scaffold systems are presented (Figs. 1–3). In general it is apparent that cytokine release from these hydrogel scaffolds was largely affected by the relative scaffold and protein charge, as well as protein molecular weight. Slightly negatively charged VEGF release from RADA16-I was suppressed compared to both positively charged βFGF and BDNF, as illustrated in the general release profile (Fig. 1) and the subsequently determined apparent diffusivity values (Table 2).

VEGF apparent diffusivity values were order of magnitude slower than both positively charged cytokines for release from RADA16-I. Despite the fact that RADA16-I has a net neutral charge at pH7.4, a potential for charge separation along the nanofiber has been shown to exist [9] due to the fact that the guanidinium group of the arginine side chain extends farther from the nanofiber surface than the neighboring carboxylic acid group of aspartic acid. It was previously determined [9] using small molecules that the access to the negatively charged aspartic acid within the nanofiber was significantly inhibited, whereas access to the positively charged arginine played a dramatic role in dictating small molecule release from RADA16-I hydrogels. As the guanidinium group has a pKa of 12.48, it readily adopts a positive charge in almost all environments. The presence of a high density of these positively charged guanidinium groups along the nanofiber surface has recently been shown to play a critical role in dictating the release of small negatively charged molecules from RADA16-I [9]. The results shown in Fig. 1 suggest that the release of negatively charged VEGF from RADA16-I is slower compared to cytokines of somewhat similar molecular weight but opposite charge, suggesting that VEGF

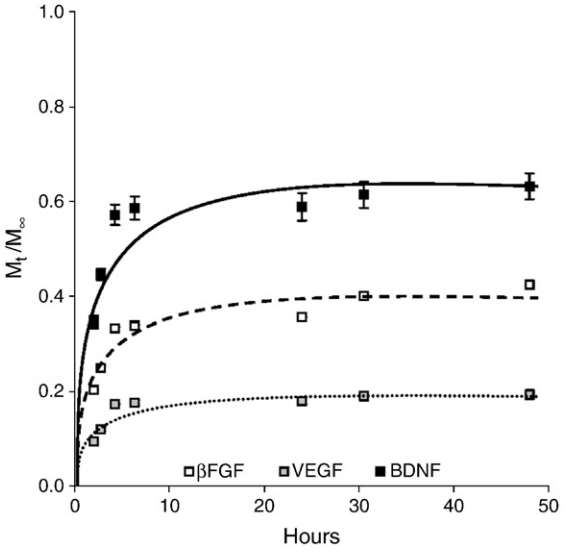

Fig. 1. Cytokine release profiles from hydrogels composed of RADA16-I. βFGF (□), VEGF (▣) and BDNF (■) were released from RADA16-I hydrogels for up to 48 h. It is evident that VEGF was released slower than the other protein systems, whereas βFGF and BDNF were slightly separated in their release rates and amounts. Data represent average value ± 1 SD, $n>5$. Note that lines are to guide the eye, and do not represent modeling results.

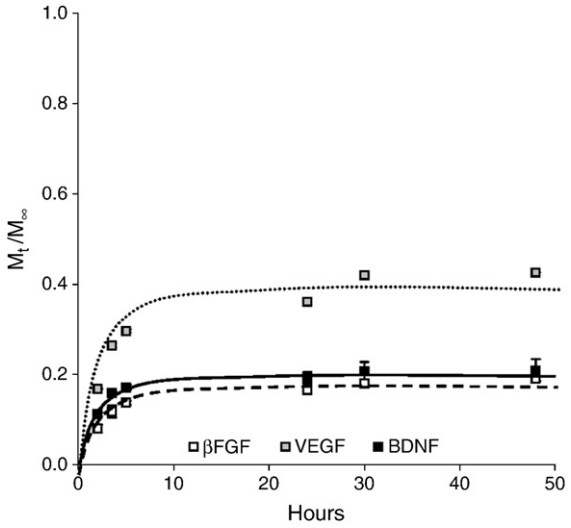

Fig. 2. Cytokine factor release profiles from hydrogel scaffolds composed of RADA16-DGE. βFGF (□), VEGF (▣) and BDNF (■) were released from RADA16-DGE hydrogel scaffold for up to 48 h. βFGF and BDNF were similar in their release rates and amounts and suppressed compared to VEGF. Data represent average value ± 1 SD, $n>5$. Note that lines are to guide the eye, and do not represent modeling results.

mobility may be hindered *via* interaction with the presence of the positive guanidinium. Moreover, these results support the previous finding [9] that although there are negative carboxylic acids in the backbone of the nanofiber, they may not play a significant role in dictating the release kinetics of molecules. It is probable that these carboxylic acids are sufficiently screened, either sterically or with counterions, making them inaccessible for interaction with positively charged proteins. Trends observed in Figs. 2 and 3 further support the conclusion that charge effects are an important mechanism for the release of proteins from these hydrogel scaffolds, where VEGF release is greater than the positively charged cytokines in negatively charged RADA16-DGE, and lower in positively charged RADA16-PFS.

RADA16-DGE is comprised of RADA16-I with two negatively charged amino acids added to its C-terminus. Plateau released

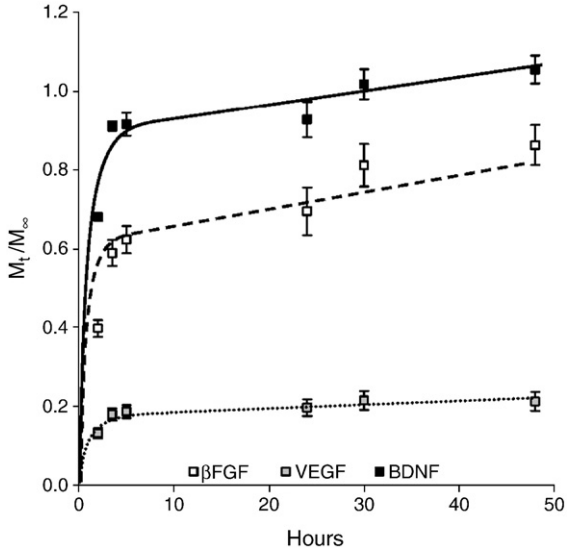

Fig. 3. Cytokine release profiles from hydrogel scaffolds composed of RADA16-PFS. βFGF (□), VEGF (▣) and BDNF (■) were released from RADA16-PFS hydrogel scaffold for up to 48 h. VEGF was released slower than the other protein systems, whereas almost all BDNF were released. βFGF release was slightly impeded in comparison to BDNF. Data represent average value ± 1 SD, $n>5$. Note that lines are to guide the eye, and do not represent modeling results.

Table 2
Apparent in-gel diffusivity ($D \times 10^{10}\,m^2/s$) values as determined from the release profile of βFGF, VEGF, and BDNF from hydrogels composed of RADA16-I, RADA16-DGE, and RADA16-PFS.

	βFGF	VEGF	BDNF
RADA16-I	0.26 ± 0.02	0.06 ± 0.01	0.77 ± 0.05
RADA16-DGE	0.039 ± 0.002	0.19 ± 0.02	0.067 ± 0.004
RADA16-PFS	0.91 ± 0.08	0.09 ± 0.01	2.2 ± 0.3

amounts (Fig. 2) and apparent diffusivity values (Table 2) showed a similar trend for βFGF, BDNF and VEGF release. The suppression of both βFGF and BDNF release from RADA16-DGE yielded apparent diffusivity values ~75% of VEGF. It is apparent that the addition of these negatively charged residues to RADA16-I reduces the release kinetics of both positively charged cytokines, when compared to RADA16-I itself. Respective plateau release amounts of βFGF and BDNF from RADA16-DGE were determined to be similar at ~0.19; this being much less than the ~0.4 and ~0.6 amounts observed in RADA16-I. These results suggest that even though the negatively charged carboxylic acids within RADA16-I seem not to interact with the positively charged cytokines, the addition of negatively charged residues to RADA16-I's C-terminus does affect protein–nanofiber interactions. Thus, the release of positively charged cytokines was greatly reduced in the RADA16-DGE system compared to the RADA16-I system. VEGF, however, has exhibited a greater plateau release amount for RADA16-DGE (~0.4) compared to RADA16-I (~0.2) systems. The increase in plateau release amount in this case may be due to the repulsive events between the negatively charged species. However, it is still apparent that the presence of these C-terminus negative residues does not provide a sufficient barrier for reducing the interaction that probably occurs between VEGF and the guanidinium groups on the RADA16-I portion of the nanofiber backbone. However, the total release observed during this time period was only ~0.4, a result that may suggest that the VEGF diffusion is hindered by the nanofibers.

RADA16-PFS is comprised of a RADA16-I segment with additional positively charged amino acids appended to the C-terminus. Plateau release amounts (Fig. 3) and apparent diffusivity values (Table 2) yield similar trends for the release of βFGF, BDNF and VEGF from RADA16-PFS; illustrating that the addition of these amino acid residues to RADA16-I facilitates the movement of positively charged species through the scaffolds. Similar to the release from RADA16-I, VEGF release from RADA16-PFS yielded apparent diffusivity values an order of magnitude lower than both positively charged cytokines. Again similar to RADA16-I data, the steady-state release of VEGF and βFGF was similar but much less than BDNF. Plateau release amounts of βFGF and BDNF increased from ~0.4 and ~0.6 in RADA16-I systems to ~0.9 and ~1 in RADA16-PFS systems, respectively. There is no significant difference between the plateau release amount of VEGF from RADA16-I and RADA16-PFS systems, both being ~0.2; thus, suggesting that the additional positive charges present on RADA16-PFS did not significantly alter the overall interaction between these nanofibers and VEGF.

Ample evidence for the effect of charge upon cytokine mobility is provided in Figs. 1–3, and it is evident that there is a difference in mobility between the positively charged βFGF and BDNF, for example, the release of βFGF is lower than BDNF for RADA16 and RADA16-PFS. A result that is discussed in more detail below.

3.2. In-gel cytokine mobility: FCS data

Despite the apparent differences in the amount and rate of released proteins as a function of charge, the underlying mechanisms responsible for this are not easily resolved. The determined apparent diffusivities derived from the release profiles cannot further elucidate the mechanisms by which molecules move through the scaffold. FCS techniques were employed in order to observe the dynamic

motion of the molecules within the peptide nanofiber scaffolds *in situ*. As we are investigating molecules moving in a complex hydrogel, changes in translational diffusion time (τ_D) can occur as a result of several events: protein aggregation, weak protein–nanofiber interactions, and path-length differences within the confocal volume due to steric effects of nanofibers. Therefore, any event that increases the time it takes the molecule to traverse the confocal volume should increase τ_D, and thus decrease the observed diffusivity value. Previous work has shown, for 1.5% (w/v) agarose gels, that diffusion of non-interacting solutes can be characterized by models that account for a combination of obstruction due to cylindrical cells and local hydrodynamics within the hydrogel [34]. It has also been shown that for interacting spheres traversing a network of very long and thin rods of cholesteric liquid crystal molecules that their diffusion is related to the tracer size relative to the network mesh-size and that both hydrodynamic and rod-sphere interactions further dictate tracer mobility [37,38].

Given the variety of known constraints, we reasoned that through choosing tracer proteins of similar sizes it would be possible to isolate and investigate charge effects on in-gel diffusivity. Table 1 illustrates the effectiveness of the FCS technique, as well as the effect of molecular crowding on protein diffusion. Using pure protein solutions ranging in concentration from 0.5 nM to 14 nM, it was possible to characterize all proteins as being a single population of diffusants, with diffusivities ranging from 1.4 to 2.2×10^{-10} m^2/s, respectively.

It is important to point out that FCS techniques only provide information about the mobile population of molecules; immobile proteins cannot be characterized and do not influence the diffusivity values. Table 3 details the average in-gel diffusivity and fraction for all populations of mobile cytokines at two points of time (2 and 48 h) during release. In general, after 2 h of release, all systems were described as having two populations of mobile fractions with different τ_D values and population fractions; exceptions include the mobility of VEGF in RADA16-I and BDNF in RADA16-PFS, which were characterized as a single population of diffusing species. For this time point, it is apparent that multi-scale diffusion events occur within most nanofiber scaffolds, most likely a result of: 1) cytokines that are 'freely' diffusing through the aqueous phase of the hydrogel; and 2) 'hindered' diffusion that is a combination of charge effects between cytokines and nanofibers as well as steric effects due to protein size. After 48 h of release, it was observed that the majority of systems could be characterized as a single population of diffusing molecules; the exception being βFGF diffusion in RADA16-I. The disappearance of the slower population of diffusing molecules may indicate that cytokines, which were hindered in their motion have either become immobilized on the nanofiber (and thus not measured), or have been freed from the nanofiber into the 'aqueous' phase of the 1 wt.% peptide nanofiber scaffolds. Moreover, it is apparent that FCS diffusivity values for all 3 cytokines were dissimilar to the apparent diffusivity values listed in Table 2. Rather, it was possible to measure the subpopulations of diffusing molecules using the FCS technique.

Cytokine diffusion within RADA16-I (Table 3) shows that after 2 h of release the positively charged βFGF and BDNF have a significant fraction (~86%) that has a similar mobility. These data suggest that this fraction of molecules was traversing the nanofiber scaffolds through the aqueous phase. The remaining fraction (~14%) of mobile βFGF and BDNF exhibits diffusivity values two orders of magnitude less than the first fraction, suggesting that these molecules may be hindered in their diffusion through the scaffold either by interaction with nanofibers, or *via* steric effects. After 48 h of release it is apparent that all BDNF molecules were moving within the aqueous phase of the hydrogel. The relative fraction of βFGF interacting with the nanofiber increased from ~14 to 40% from 2 to 48 h. This increase in the population of molecules experiencing hindered diffusion may result from the decreasing concentration of βFGF in the local aqueous phase only. However, it should be noted that the counting statistics for this data set were low and may lead to a low confidence in this value. βFGF and BDNF mobility was drastically greater than that of the negatively charged VEGF within RADA16-I, which was characterized by a single population of mobile proteins with a diffusivity of ~0.38×10^{-10} m^2/s. These data suggest that VEGF mobility is impeded, possibly due to its interaction with the nanofibers of the nanofiber scaffold, and that the diffusivity value represents the general mobility of these molecules as they interact with the guanidinium groups along the RADA16-I nanofiber. Perhaps presenting the mechanistic reason that VEGF release, as illustrated in Fig. 1, was severely hindered compared to the release of βFGF and BDNF from RADA16-I. After 48 h of release, it was observed that VEGF diffusion was similar to the 2-hour time point.

For RADA16-DGE systems, the mobility of both positively charged cytokines (βFGF and BDNF) was significantly altered. After 2 h of release, the fraction of βFGF and BDNF with diffusivities similar to solution free molecules dropped from ~86% in RADA16-I to ~70% in RADA16-DGE, while the diffusivity values for this population also dropped from 1.79 and 2 to ~1.4×10^{-10} m^2/s. As protein concentration was similar between the two systems, these differences suggest an increase in nanofiber–protein interaction due to charge and coinciding with the overall release profiles outlined in Fig. 2. After 48 h of release, the majority of molecular transport occurs within the aqueous phase of the hydrogel. When considering the mobility of the negatively charged VEGF through the RADA16-DGE nanofiber

Table 3
Summary of in-gel mobility of 3 cytokines for 3 different hydrogel scaffolds after 2 h and 48 h of release as determined using FCS techniques. Data include population diffusivities (D) and population fractions (F). Values represent mean ± 1 SD for $n>5$.

	2-hour time point				48-hour time point			
	D_1, $\times10^{10}$ m^2/s	F_1, %	D_2, $\times10^{10}$ m^2/s	F_2, %	D_1, $\times10^{10}$ m^2/s	F_1, %	D_2, $\times10^{10}$ m^2/s	F_2, %
RADA16-I								
βFGF	1.79 ± 0.04	86 ± 4	0.032 ± 0.007	14 ± 4	1.4 ± 0.4$^{\Delta1}$	63 ± 11	0.06 ± 0.03	40 ± 10
VEGF	0.38 ± 0.02	100 ± 0	–	–	0.5 ± 0.1	100 ± 0	–	–
BDNF	2.0 ± 0.1	87 ± 3	0.09 ± 0.02	14 ± 2	2.0 ± 0.2	100 ± 0	–	–
RADA16-DGE								
βFGF	1.37 ± 0.07	71 ± 5	0.036 ± 0.006	12 ± 4	1.26 ± 0.05	100 ± 0	–	–
VEGF	1.5 ± 0.1	54 ± 5	0.28 ± 0.06	28 ± 6	1.9 ± 0.1	100 ± 0	–	–
BDNF	1.4 ± 0.1	69 ± 4	0.18 ± 0.06	16 ± 4	1.6 ± 0.3	100 ± 0	–	–
RADA16-PFS								
βFGF	1.5 ± 0.2	83 ± 8	0.19 ± 0.05	19 ± 9	1.6 ± 0.1	100 ± 0	–	–
VEGF	1.8 ± 0.4	68 ± 34	0.42 ± 0.01	8 ± 0.5	1.9 ± 0.1	100 ± 0	–	–
BDNF	1.6 ± 0.1	10 ± 0	–	–	1.8 ± 0.3	100 ± 0	–	–

Total count rate within the volume for these points was above the manufacturer's recommended minimum, except where otherwise indicated ($^{\Delta}$); model χ^2 were low at 10–30.
$^{\Delta1}$Sample count rates of ~10 kHz, model χ^2 values were ~250.

scaffold, it is apparent that addition of negatively charged residues significantly altered their in-gel mobility. After 2 h of release, a large fraction (~55%) of VEGF had mobility only slightly suppressed compared to the solution condition, whereas the remaining fraction experienced a diffusivity ~0.28×10^{-10} m^2/s, similar to that observed for VEGF in RADA16-I, suggesting that this population of VEGF may closely interact with the RADA16-I segment of the nanofibers. Also, these results may explain the mechanistic differences that resulted in the increase in both the release rate and plateau release amount of VEGF in RADA16-DGE (Fig. 2). After 48 h, it was observed that all VEGF transport occurs in the solution phase.

After 2 h of release, cytokine mobility within the positively charged RADA16-PFS nanofiber scaffold (Table 3) yielded a large fraction of βFGF and BDNF (~83 and 100, respectively) that had mobility similar to the solution values. The increase in population of βFGF and BDNF from ~70 in RADA16-DGE to >83 in RADA16-PFS is thought to be directly related to the presence of the positively charged residue appended to the RADA16-I segment of RADA16-PFS. The slower moving fraction of βFGF (~20%) has an increased diffusivity as compared to the RADA16-I situation. The diffusing populations of βFGF and BDNF were found to be solely within the solution phase of the hydrogel after 48 h of release. VEGF mobility within RADA16-PFS, after 2 h of release, yielded a system of two populations of average diffusivities of ~1.8 and ~0.4×10^{-10} m^2/s. It is apparent that the slower moving fraction of VEGF has a similar diffusivity value (~0.4×10^{-10} m^2/s) throughout all three scaffolds, suggesting that RADA16-I interactions persist throughout all experiments. This system did show a large fraction of VEGF diffusing in the solution phase, however, the relative error for both the diffusivity and the fraction reduces the confidence in these values. After 48 h of release, all mobile VEGF were located within the solution phase of RADA16-PFS. These results may suggest that the slower moving population of VEGF has partitioned into the aqueous phase within the hydrogel, or has become static upon the nanofibers.

3.3. Released cytokine mobility: FCS determined diffusivities

FCS techniques were utilized to analyze eluted cytokines so as to determine if the processes involved in incorporating and releasing them from the various nanofiber scaffolds led to changes in the state of the proteins in solution: unfolding, aggregation, etc. If aggregation or significant unfolding events occurred, it would be expected to result in a significant change in the translational diffusion time of the fluorescent molecules; thus, affecting the calculated diffusivity times. In general, after both 2 h and 48 h of release, it was observed (Table 4) that the cytokines were adequately described as a single population of diffusing molecules with diffusivities similar to that determined experimentally (FCS) for native cytokines in solution (Table 1). VEGF release from RADA16-I was characterized as having equal fractions with mobilities similar to native VEGF and a significantly slower diffusion rate.

Although it is difficult to determine the mechanism for these populations of molecules diffusing at a slower rate, it is apparent that: 1) there were a large fraction of VEGF that didn't have their mobility altered compared to native VEGF; and 2) that the slower moving fraction of VEGF did not coincide with the in-gel diffusivity values: thus not representing the diffusing population within the hydrogel scaffolds. The observed diffusivity values were half that of the solution free VEGF, it is most likely that some VEGF may have formed aggregates. A similar trend has been observed for βFGF released from RADA16-PFS; however, it is evident that aggregate formation is only a small fraction (~15%) of the released βFGF.

After 48 h, the concentration of released protein released was low, resulting in low counting statistics. In particular, VEGF release from RADA16-I and RADA16-DGE showed populations of low diffusivity values. In both cases, however, the counting rates were very low compared to other solutions. However, it is possible that VEGF may also have formed aggregates upon release from RADA16-DGE as we see that the slower population was half that of the solution free population.

3.4. Mechanistic differences between βFGF and BDNF mobility

Both the release kinetics and plateau released amounts of βFGF were less than BDNF for scaffolds of positive charge (Figs. 1 and 3, Table 3). Respective apparent diffusivities from the solution data for βFGF and BDNF in RADA16-I and RADA16-PFS were ~0.26 and 0.77, and ~0.91 and 2.2×10^{-10} m^2/s. Respective plateau values for βFGF and BDNF in RADA16-I and RADA16-PFS were ~0.4 and 0.6, and 0.9 and 1. Although it might be expected that the slightly larger BDNF should diffuse slower through the scaffold, these data suggest the opposite. This difference in release rate and plateau released amounts may indicate that βFGF takes a longer path through the scaffold. Molecular size differences between βFGF and BDNF coupled with the fact that these nanofiber scaffolds contain nanopores of ~5–200 nm [39] make it plausible that βFGF is able to traverse a larger population of nanopores within the scaffold; thereby significantly increasing the path length required to move through the nanofiber scaffolds,

Table 4
Post-elution mobility of 3 cytokines in 3 different scaffolds after 2 h and 48 h of release as determined using FCS techniques. Data include population diffusivities (D) and population fractions (F). Values represent mean ± 1 SD for $n>5$.

	2-hour time point				48-hour time point			
	D_1, $\times10^{10}$ m^2/s	F_1, %	D_2, $\times10^{10}$ m^2/s	F_2, %	D_1, $\times10^{10}$ m^2/s	F_1, %	D_2, $\times10^{10}$ m^2/s	F_2, %
RADA16-I								
βFGF	1.92 ± 0.14	100	–	–	1.8 ± 0.2	100	–	–
VEGF	1.4 ± 0.2	59 ± 11	0.67 ± 0.03	49 ± 25	09 ± 0.1$^{\Delta2}$	61 ± 20	0.3 ± 0.1	20 ± 5
BDNF	2.10 ± 0.05	100	–	–	2.1 ± 0.3	100	–	–
RADA16-DGE								
βFGF	1.7 ± 0.1	100	–	–	1.5 ± 0.2	100	–	–
VEGF	1.3 ± 0.1	100	–	–	1.2 ± 0.3$^{\Delta1}$	47 ± 10	0.6 ± 0.08	52 ± 15
BDNF	1.78 ± 0.06	100	–	–	1.7 ± 0.3	100	–	–
RADA16-PFS								
βFGF	1.98 ± 0.30	68 ± 15	0.7 ± 0.1	15 ± 7	1.6 ± 0.2	100	–	–
VEGF	1.99 ± 0.04	100	–	–	1.9 ± 0.2	100	–	–
BDNF	1.86 ± 0.05	100	–	–	1.6 ± 0.3	100	–	–

Total count rate within the sample volume for these points were above the manufacturer's recommended minimum, except where otherwise indicated ($^{\Delta}$); model χ^2 were low at 10–30.
$^{\Delta1}$ Sample count rates of ~30 kHz, model χ^2 values were~100.
$^{\Delta2}$ Sample count rates of ~10 kHz, model χ^2 values were~100.

leading to a lowering of the apparent diffusivity and plateau released amounts. Therefore, there is not only evidence to show that charge effects play a crucial role in dictating the mobility of proteins within these scaffolds, but that steric effects are also present.

3.5. Released cytokine activity: cell assays

BDNF was not tested for the cell proliferation assays because it intrinsically lacks a potential mitogenic effect for our experimental cell phenotypes. βFGF has been proven as an important mitotic agent capable of actively stimulating neural stem cell proliferation [40]. To assess the activity of the released βFGF from the designer self-assembling peptide scaffolds it was released from RADA16-I and RADA16-DGE scaffolds, where it was shown to significantly stimulate NSC proliferation for up to three weeks (compared with negative control—Welch's unpaired *t*-test: week I RADA16-I $P=0.0021$, RADA16-DGE $P=0.0011$; week II RADA16-I $P<0.0001$, RADA16-DGE $P<0.0001$; week III RADA16-I $P<0.0001$, RADA16-DGE $P=0.0009$). MTT assay (Fig. 4) shows incremented NSC progeny while daily optical screening of cultured NSCs confirmed the formation of neurospheres, usually found in NSCs floating culture conditions, mainly in the case of RADA16-I and RADA16-DGE scaffolds. In case of RADA16-PFS NSC

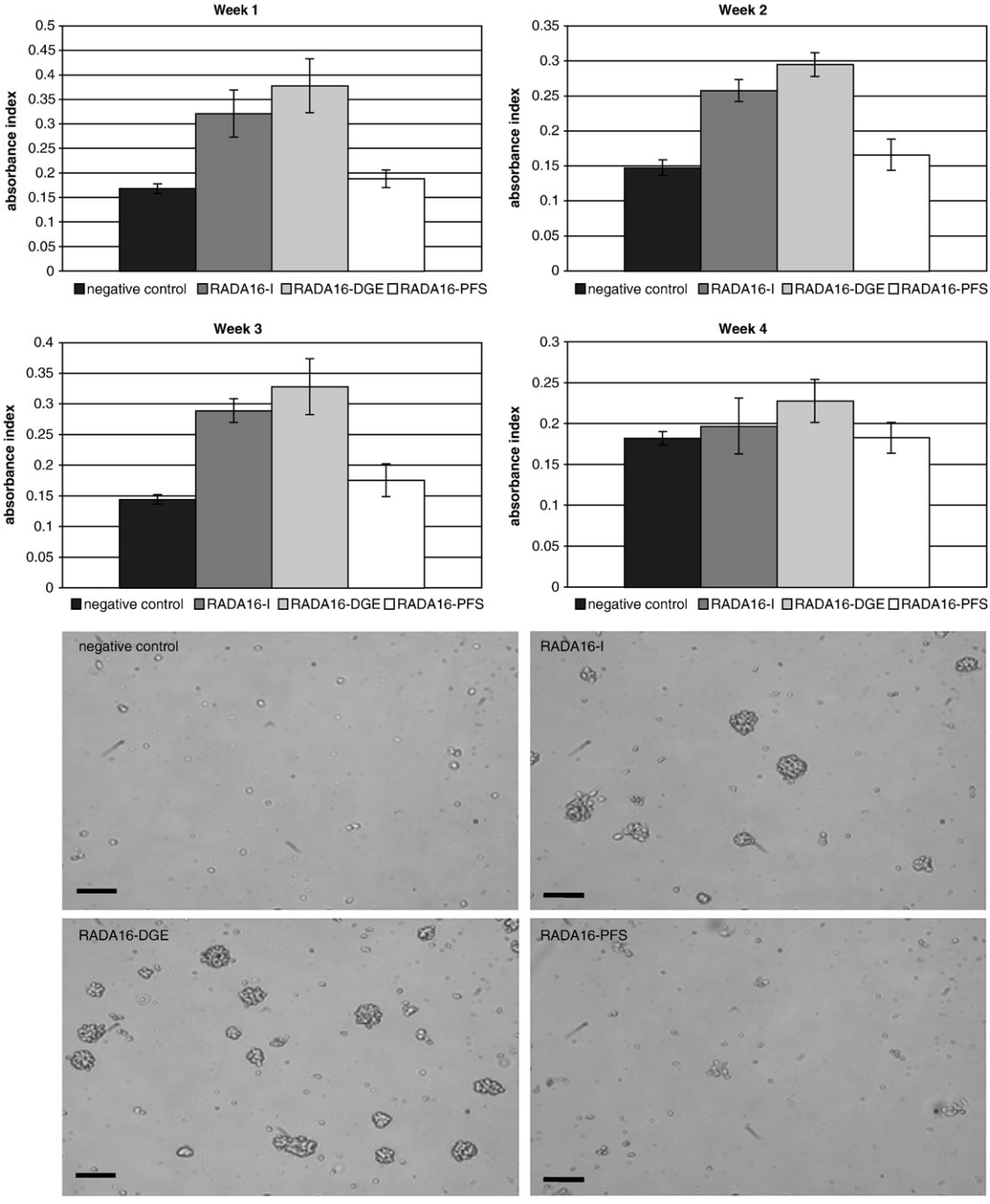

Fig. 4. Proliferation effect of released βFGF over neural stem cells. A) MTT assay for proliferated progeny ($n=5$). In the case of RADA16-I and RADA16-DGE a long-term effect of released βFGF is evidenced by significantly higher total cell population. The βFGF mitogenic activity can be appreciated till four weeks after mixing the GF with the self-assembling scaffolds. Data represent average values ± 1 SD. B) Week 2 of *in vitro* GF release. NSCs were replaced with newly dissociated cells at the end of week 1 (see Materials and methods for details). Micrographs of proliferated NSCs at week 2 day 7 of βFGF release. Neurospheres testify an NSC proliferation in the case βFGF released from RADA16-I and RADA16-DGE scaffolds. In RADA16-PFS cells amount does not differ from the negative controls both in its MTT values and *via* microscope imaging. Scale bars 50 μm.

population did not differ significantly from negative controls. *In vitro* results are in accordance with plateau release amounts obtained till 48 h, where RADA16-DGE, RADA16-I and RADA16-PFS showed values of 0.19, 0.4 and 0.9, respectively. Given the asymptotic release of βFGF from each peptide scaffold after the initial burst within the first 6 h we can reasonably assume a similar release for additional days if the overall systems are not perturbed and the balance between the released and the loosely bound GFs is not in equilibrium. The initial burst can also be regulated with addition of another layer outside of the scaffold to contain it. This finding suggests that the release of active βFGF is likely to persist over several weeks till the reservoir of the slower diffusing cytokine interacting with the electrostatic charges of the assembled nanofibers is over. These findings may be useful for *in vivo* long-term release of βFGF to enhance the vascularization of engineered implanted tissues *via* non-invasive and applicable devices [41–43].

A similar experimental setup using a MTT proliferation assay with mouse endothelial cells exposed to the slow release of VEGF provided *in vitro* results in accordance with the FC section findings (results not shown). However we detected differences in the proliferation of the endothelial cell populations versus the peptide scaffolds tested. Nonetheless significant differences lasted for two weeks. We assume this finding may be given by a sensitivity of endothelial cells to the proliferative stimulus brought by VEGF released in the supernatant at low concentration.

4. Conclusion

Controlling the cellular microenvironment *via* controlling the presentation of functional cytokines to local cells is crucial to the design of biomaterials for regenerative medicine strategies. The engineering of RADA16-I self-assembling peptides may provide a means for further understanding how the physicochemical environment affects protein mobility within gels. We report that designer self-assembling peptide scaffolds facilitate slow and sustained release of active cytokines, whereby mobile molecules are found to be within the bulk aqueous fraction and a 'hindered' fraction within RADA16-I RADA16-DGE and RADA16-PFS nanofiber system. Functional βFGF and VEGF release is observed to occur over 2 to 3 weeks. With our systematic experiments, and new findings, new self-assembling peptide nanofiber scaffolds for a wide range of therapeutically important scaffolds will be designed.

Acknowledgements

The authors would like to acknowledge Sotirios Koutsopoulos for initial discussions. FG gratefully acknowledges Angelo Vescovi for his helpful advice, Omar Villa for his contribution in AFM imaging, CARIPLO foundation and Regione Lombardia for funding the research involved in this work. LDU gratefully acknowledges financial support from the National Research Council-Canada. SZ gratefully acknowledges funding in part by a grant from NIH-BRP EB003805.

Appendix A. Supplementary data

Supplementary data associated with this article can be found, in the online version, at doi:10.1016/j.jconrel.2010.04.026.

References

[1] A.S. Hoffman, Hydrogels for biomedical applications, Adv. Drug Deliv. Rev. 54 (1) (2002) 3–12.
[2] Q. Hou, P.A. De Bank, K.M. Shakesheff, Injectable scaffolds for tissue regeneration, J. of Mat. Chem. 4 (12) (2004) 8.
[3] J. Elisseeff, Injectable cartilage tissue engineering, Expert Opin. Biol. Ther. 4 (12) (2004) 1849–1859.
[4] S. Zhang, Fabrication of novel biomaterials through molecular self-assembly, Nat. Biotechnol. 21 (10) (2003) 1171–1178.
[5] S. Ramachandran, Y.B. Yu, Peptide-based viscoelastic matrices for drug delivery and tissue repair, BioDrugs 20 (5) (2006) 263–269.
[6] V.F. Segers, R.T. Lee, Local delivery of proteins and the use of self-assembling peptides, Drug Discov. Today 12 (13–14) (2007) 561–568.
[7] M.E. Davis, J.P. Motion, D.A. Narmoneva, T. Takahashi, D. Hakuno, R.D. Kamm, S. Zhang, R.T. Lee, Injectable self-assembling peptide nanofibers create intramyocardial microenvironments for endothelial cells, Circulation 111 (4) (2005) 442–450.
[8] S. Zhang, C. Lockshin, R. Cook, A. Rich, Unusually stable beta-sheet formation in an ionic self-complementary oligopeptide, Biopolymers 34 (5) (1994) 663–672.
[9] Y. Nagai, L.D. Unsworth, S. Koutsopoulos, S. Zhang, Slow release of molecules in self-assembling peptide nanofiber scaffold, J. Control. Release 115 (1) (2006) 18–25.
[10] R.G. Ellis-Behnke, Y.X. Liang, S.W. You, D.K. Tay, S. Zhang, K.F. So, G.E. Schneider, Nano neuro knitting: peptide nanofiber scaffold for brain repair and axon regeneration with functional return of vision, Proc Natl Acad Sci U S A 103 (13) (2006) 5054–5059.
[11] F. Gelain, D. Bottai, A. Vescovi, S. Zhang, Designer self-assembling peptide nanofiber scaffolds for adult mouse neural stem cell 3-dimensional cultures, PLoS ONE 1 (2006) e119.
[12] A. Horii, X. Wang, F. Gelain, S. Zhang, Biological designer self-assembling peptide nanofiber scaffolds significantly enhance osteoblast proliferation, differentiation and 3-D migration, PLoS ONE 2 (2) (2007) e190.
[13] G.A. Silva, C. Czeisler, K.L. Niece, E. Beniash, D.A. Harrington, J.A. Kessler, S.I. Stupp, Selective differentiation of neural progenitor cells by high-epitope density nanofibers, Science 303 (5662) (2004) 1352–1355.
[14] V.M. Tysseling-Mattiace, V. Sahni, K.L. Niece, D. Birch, C. Czeisler, M.G. Fehlings, S.I. Stupp, J.A. Kessler, Self-assembling nanofibers inhibit glial scar formation and promote axon elongation after spinal cord injury, J. Neurosci. 28 (14) (2008) 3814–3823.
[15] M.E. Davis, P.C. Hsieh, T. Takahashi, Q. Song, S. Zhang, R.D. Kamm, A.J. Grodzinsky, P. Anversa, R.T. Lee, Local myocardial insulin-like growth factor 1 (IGF-1) delivery with biotinylated peptide nanofibers improves cell therapy for myocardial infarction, Proc Natl Acad Sci U S A 103 (21) (2006) 8155–8160.
[16] D.A. Narmoneva, O. Oni, A.L. Sieminski, S. Zhang, J.P. Gertler, R.D. Kamm, R.T. Lee, Self-assembling short oligopeptides and the promotion of angiogenesis, Biomaterials 26 (23) (2005) 4837–4846.
[17] S. Koutsopoulos, L.D. Unsworth, Y. Nagai, S. Zhang, Controlled release of functional proteins through designer self-assembling peptide nanofiber hydrogel scaffold, Proc Natl Acad Sci U S A 106 (12) (2009) 4623–4628.
[18] A. Schanzer, F.P. Wachs, D. Wilhelm, T. Acker, C. Cooper-Kuhn, H. Beck, J. Winkler, L. Aigner, K.H. Plate, H.G. Kuhn, Direct stimulation of adult neural stem cells *in vitro* and neurogenesis *in vivo* by vascular endothelial growth factor, Brain Pathol. 14 (3) (2004) 237–248.
[19] M. Zhang, I.V. Yannas, Peripheral nerve regeneration, Adv. Biochem. Eng. Biotechnol. 94 (2005) 67–89.
[20] B. Bjellqvist, G.J. Hughes, C. Pasquali, N. Paquet, F. Ravier, J.C. Sanchez, S. Frutiger, D. Hochstrasser, The focusing positions of polypeptides in immobilized pH gradients can be predicted from their amino acid sequences, Electrophoresis 14 (10) (1993) 1023–1031.
[21] J. Crank, G.S. Park, Diffusion in Polymers, Academic Press, New York, 1968.
[22] N. Vahdat, V.D. Sullivan, Estimation of permeation rate of chemicals through elastometric materials, J. of Appl. Polymeric Sci. 79 (2001) 8.
[23] J. Siepmann, A. Ainaoui, J.M. Vergnaud, R. Bodmeier, Calculation of the dimensions of drug-polymer devices based on diffusion parameters, J. Pharm. Sci. 87 (7) (1998) 827–832.
[24] M. Wachsmuth, W. Waldeck, J. Langowski, Anomalous diffusion of fluorescent probes inside living cell nuclei investigated by spatially-resolved fluorescence correlation spectroscopy, J. Mol. Biol. 298 (4) (2000) 677–689.
[25] I.M. Sokolov, J. Klafter, From diffusion to anomalous diffusion: a century after Einstein's Brownian motion, Chaos 15 (2) (2005) 26103.
[26] M.C. Branco, D.J. Pochan, N.J. Wagner, J.P. Schneider, Macromolecular diffusion and release from self-assembled beta-hairpin peptide hydrogels, Biomaterials 30 (7) (2009) 1339–1347.
[27] J.J. Panda, A. Mishra, A. Basu, V.S. Chauhan, Stimuli responsive self-assembled hydrogel of a low molecular weight free dipeptide with potential for tunable drug delivery, Biomacromolecules 9 (8) (2008) 2244–2250.
[28] G. Liang, Z. Yang, R. Zhang, L. Li, Y. Fan, Y. Kuang, Y. Gao, T. Wang, W.W. Lu, B. Xu, Supramolecular hydrogel of a D-amino acid dipeptide for controlled drug release *in vivo*, Langmuir 25 (15) (2009) 8419–8422.
[29] J. Enderlein, I. Gregor, D. Patra, T. Dertinger, U.B. Kaupp, Performance of fluorescence correlation spectroscopy for measuring diffusion and concentration, Chemphyschem 6 (11) (2005) 2324–2336.
[30] W.W. Webb, Fluorescence correlation spectroscopy: inception, biophysical experimentations, and prospectus, Appl. Opt. 40 (24) (2001) 3969–3983.
[31] R. Rigler, E. Elson, Fluorescence Correlation Spectroscopy: Theory and Applications, Springer, New York, 2001.
[32] M.J. Saxton, Anomalous diffusion due to binding: a Monte Carlo study, Biophys. J. 70 (3) (1996) 1250–1262.
[33] J.F. Nagle, Long tail kinetics in biophysics? Biophys. J. 63 (2) (1992) 366–370.
[34] N. Fatin-Rouge, K. Starchev, J. Buffle, Size effects on diffusion processes within agarose gels, Biophys. J. 86 (5) (2004) 2710–2719.
[35] A. Gritti, E.A. Parati, L. Cova, P. Frolichsthal, R. Galli, E. Wanke, L. Faravelli, D.J. Morassutti, F. Roisen, D.D. Nickel, A.L. Vescovi, Multipotential stem cells from the adult mouse brain proliferate and self-renew in response to basic fibroblast growth factor, J. Neurosci. 16 (3) (1996) 1091–1100.
[36] F. Taraballi, M. Campione, A. Sassella, A. Vescovi, A. Paleari, W. Hwang, F. Gelain, Effect of functionalization on the self-assembling propensity of beta-sheet forming peptides, Soft Matter 5 (3) (2009) 660–668.

[37] K. Kang, J. Gapinski, M.P. Lettinga, J. Buitenhuis, G. Meier, M. Ratajczyk, J.K. Dhont, A. Patkowski, Diffusion of spheres in crowded suspensions of rods, J Chem Phys 122 (4) (2005) 44905.
[38] K. Kang, A. Wilk, J. Buitenhuis, A. Patkowski, J.K. Dhont, Diffusion of spheres in isotropic and nematic suspensions of rods, J Chem Phys 124 (4) (2006) 044907.
[39] S. Zhang, T. Holmes, C. Lockshin, A. Rich, Spontaneous assembly of a self-complementary oligopeptide to form a stable macroscopic membrane, Proc Natl Acad Sci U S A 90 (8) (1993) 3334–3338.
[40] A.L. Vescovi, A. Gritti, R. Galli, E.A. Parati, Isolation and intracerebral grafting of nontransformed multipotential embryonic human CNS stem cells, J. Neurotrauma 16 (8) (1999) 689–693.
[41] K.G. Marra, A.J. Defail, J.A. Clavijo-Alvarez, S.F. Badylak, A. Taieb, B. Schipper, J. Bennett, J.P. Rubin, FGF-2 enhances vascularization for adipose tissue engineering, Plast. Reconstr. Surg. 121 (4) (2008) 1153–1164.
[42] W. Ryu, Z. Huang, F.B. Prinz, S.B. Goodman, R. Fasching, Biodegradable micro-osmotic pump for long-term and controlled release of basic fibroblast growth factor, J. Control. Release 124 (1–2) (2007) 98–105.
[43] S. Nakamura, M. Nambu, T. Ishizuka, H. Hattori, Y. Kanatani, B. Takase, S. Kishimoto, Y. Amano, H. Aoki, T. Kiyosawa, M. Ishihara, T. Maehara, Effect of controlled release of fibroblast growth factor-2 from chitosan/fucoidan micro complex-hydrogel on *in vitro* and *in vivo* vascularization, J. Biomed. Mater. Res. A 85 (3) (2008) 619–627.